Journal of Materials Chemistry A

Accepted Manuscript

ROYAL SOCIETY OF CHEMISTRY

www.rsc.org/materialsA

Journal Name

RSCPublishing

ARTICLE

Ultrasonic-Assisted Synthesis of Bimetallic PtRu Nanoparticles Supported on Carbon Nanotubes for Effective Methanol Oxidation

Cite this: DOI: 10.1039/x0xx00000x

Received 00th January 2012,
Accepted 00th January 2012

DOI: 10.1039/x0xx00000x

www.rsc.org/

Yazhou Zhou,[‡ ab] Guohai Yang,[‡b] Horng Bin Pan,[c] Chengzhou Zhu,[b] Shaofang Fu,[b] Qiurong Shi,[b] Dan Du,[b] Xiaonong Cheng,[a] Juan Yang,[*a] Chien M. Wai,[c] and Yuehe Lin[*b]

In this paper, we demonstrate a facile and one-step ultrasonic method to synthesize the bimetallic platinum ruthenium nanoparticles supported by carboxylate functionalized multi-walled carbon nanotubes (PtRu/c-MWNTs) catalyst. The results show that the atomic Pt:Ru ratio is approximately 1:1, and the Pt mass loading in catalyst is 8 %. In addition, PtRu nanoparticles with bimetallic structure, ultrasmall size (1.9 nm), and uniform distribution were well-dispersed onto the surface of c-MWNTs, which exhibit enhanced electrocatalytic performance toward methanol oxidation. It is found that this catalyst has much higher electrochemical active surface area (ECSA) (133.2 m^2 g_{Pt}^{-1}) and current density for methanol oxidation (1236.0 mA mg_{Pt}^{-1}) than those of commercial Pt/C (20 wt.%) (55.6 m^2 g_{Pt}^{-1}, 214.2 mA mg_{Pt}^{-1}). Furthermore, the oxidation current density of PtRu/c-MWNTs catalyst at 10000 s is 22.5 mA mg_{Pt}^{-1}, which indicates a long-term high electrocatalytic activity of PtRu/c-MWNTs catalyst for methanol oxidation in acid media.

1. Introduction

Direct methanol fuel cells (DMFCs), one type of the direct fuel cells, using liquid methanol as a fuel have been viewed as candidates for the dominant energy conversion devices in future applications because methanol is the next best fuel in terms of energy densities after hydrogen.[1-3] In addition, methanol offers certain specific advantages over hydrogen, such as: cheap, plentiful, renewable, and easily stored, transported, and distributed.[4] However, the drawbacks of anode platinum (Pt) electrocatalysts, such as slow kinetics,[5] low efficiency,[6] high methanol crossover,[7] scarcity and high cost of Pt,[8,9] hinder a widespread commercialization of these fuel cells. Furthermore, the electrocatalytic performance of Pt degrades quickly because of the partial blocking of the Pt surface by CO-like intermediates at low temperature, which results in a decrease of methanol oxidation currents.[1,10] Therefore, current research still focuses on development of catalysts that exhibit high electrocatalytic performance, tolerance to CO poisoning, and high stability, and are inexpensive.

To achieve the desired performance of catalysts for methanol oxidation, Pt has been modified by a second or a third metal[11,12] or forming core–shell,[3,14] dendritic nanostructure, [15,16] porous structure,[17] metal oxide,[18,19] and so on. In this context, Pt-Ru alloy nanoparticles supported on carbon substrates catalysts have shown to be one of the best catalysts for the methanol electrooxidation reaction.[20] Introduction of Ru in catalysts can not only overcome the poisoning of active sites by CO, but also reduce the cost by reduction of Pt loading level.[21] One of the major hurdles for wide applications of Pt-Ru supported on carbon substrate catalysts lies on the difficulty in reduction of Pt loading levels by an order of magnitude or two while maintaining the activity at the same or improved levels.[1] This study aims to explore a facile and one-step synthetic strategy for fabrication of bimetallic PtRu supported on carbon nanotubes catalysts with low Pt loading level and high electrocatalytic activity toward methanol oxidation through ultrasonic technique.

Ultrasonic technique, since discovered, has been studied for producing different kinds of nanomaterials, especially noble metal or bimetallic nanoparticles.[22] During the irradiation of liquids with ultrasonic, the extreme but transient local

conditions caused by acoustic cavitation (~5000 K, ~500 bar) can not only synthesize nanoparticles with small size and narrow distribution but can also facilitate the uniform deposition of the nanoparticles onto another supports or substrates.[23] It is well known that the typical parameters to tailor the catalytic performance of bimetallic catalysts are morphology, size, distribution and metal atomic ratio, and dispersibility on supports.[24] Thus, in this paper, we introduce a facile and one-step method for using ultrasonic to assist the synthesis of a catalyst combined with bimetallic PtRu nanoparticles and carboxylate functionalized multi-walled carbon nanotubes (PtRu/c-MWNTs). This catalyst has a low Pt loading (8 %), but its electrocatalytic activity toward methanol oxidation is much higher than that of commercial Pt/C (20 wt.%) catalyst. Furthermore, outstanding tolerance to CO poisoning and stability toward methanol oxidation were also exhibited by this catalyst. The excellent performance of the catalyst could probably be attributed to bimetallic structure, ultrasmall size and uniform distribution of PtRu nanoparticles, and good dispersibility onto the surface of carbon nanotubes.

2. Experimental Section

2.1 Reagents and Materials

Ruthenium (III) chloride trihydrate ($RuCl_3 \cdot 3H_2O$), and potassium tetrachloroplatinate (II) (K_2PtCl_4) were purchased from Strem Chemicals Inc. Borane morpholine complex was purchased from Alfa Aesar. Carboxylic acid functionalized multiwalled carbon nanotubes (c-MWNTs) (10-30 nm in diameter) with purity of 95 % were obtained from Nanostructured & Amorphous Materials Inc., USA. Sulfuric acid, methanol, Nafion (5 mass %) were all purchased from Sigma-Aldrich. Commercial platinum/carbon (Pt/C) (Pt loading: 20 wt.%, Pt on carbon black) was purchased from Alfa Aesar.

2.2 Synthesis of PtRu/c-MWNT catalysts

For ultrasonic synthesis of PtRu/c-MWNT catalysts, a mechanical ultrasonic cleaner bath FS60H (Fisher Scientific, USA) was employed for continuous sonication. For a typical procedure, 20 mg of c-MWNTs were charged in a 50 mL flask containing 20 mL ethanol and the solution was sonicated for 1 h to disperse the c-MWNTs. And then well-dispersed c-MWNTs solution was added with 400 μL of an aqueous solution of mixing 0.1 M $K_2PtCl_{4(aq)}$ and 0.1 M $RuCl_{3(aq)}$ (1 : 1 molar ratio of Pt^{2+} and Ru^{3+} ions). 40 mg of borane morpholine complex reducing agent was added into the c-MWNT complex solution and then the system was continually sonicated for another 20 min. Finally, the product was separated by centrifugation, washed with ethanol several times and dried at 60 ^oC for 12 h in an oven, and labeled as PtRu/c-MWNT. The Pt/c-MWNTs and Ru/c-MWNTs were synthesized using the same procedures by reduction of 0.1 M K_2PtCl_4(aq) (400 mL) and 0.1 M $RuCl_3$(aq) (400 mL) aqueous solution, respectively.

2.3 Characterization

Transmission electron microscope (TEM) measurements of samples were carried out using a JEM-1200EX II with a field emission source, and the accelerating voltage was 120 kV. X-ray photoelectron spectroscopy (XPS) was performed using a Kratos AXIS-165 with a monochromatized AlKα X-ray anode (1486.6 eV). Energy dispersive X-ray spectrometric (EDX) experiments were carried out on an AMRAY 1830, HITACHIS-2300 scanning electron microscope (SEM). The X-ray diffraction (XRD) analyses were performed on a Siemens D5000 powder X-ray diffractometer with Cu KR radiation at 40 kV and 30 mA. The actual metal loading was analyzed by inductively coupled plasma atomic emission spectroscopy (ICP-AES) (Thermo-Fisher iCAP 6300, Thermo Fisher Scientific Inc.).

2.4 Electrocatalytic Activity Measurements

The electrochemical tests were carried out in a standard three electrode system controlled with a CHI 630E station (CH Instruments, Inc., USA) with Pt wire and Ag/AgCl as the counter electrode and reference electrode, respectively. The working electrodes were prepared by applying catalyst ink onto the republished glass carbon disk electrodes. In brief, the as-prepared electrocatalyst was dispersed in isopropanol (99.5 %), Nafion (5 %), water (V/V/V: 2/8/0.05) and ultrasonicated to form a uniform catalyst ink (2 mg mL^{-1}). A total of 10 μL of well dispersed catalyst ink was applied onto the pre-polished glassy carbon (GC) disk electrode (3 mm in diameter). The well-prepared electrodes were dried at 60 ^oC for 30 min before the electrochemical tests. For comparisons, catalytic performance of the Pt/c-MWNTs and commercial Pt/C (20 wt. % Pt) were also investigated under the same condition. In addition, all the samples are uniformly dispersed on the GC disk electrodes and the coverage is almost the same for the two samples. Separate electrochemical CO stripping experiments were employed to evaluate the electrocatalyst surface area specific to CO sorption. The electrode was first cleaned by scanning 20 cycles between -0.2 and 1.2 V in N_2-saturated 0.5 M H_2SO_4 at 50 mV s^{-1}. The electrode potential was then held at 0.6 V vs. Ag/AgCl in a CO-saturated 0.5 M H_2SO_4 solution for 30 min to enable equilibration of CO adsorption on the surface of the electrocatalyst. The solution was subjected to N_2 purging for 30 min with the electrode. Finally, CO stripping voltammograms were recorded for the CO-sorbed electrode from -0.2 V to 1.2 V at a scan rate of 50 mV s^{-1}.

3. Results and discussion

3.1 Characterization of PtRu/c-MWNT catalyst

In our previous work,[25] the ultrasonic assisted method to synthesize the CNTs-supported metallic nanoparticles catalysts involves two crucial aspects: (a) functionalized MWNTs by carboxylate groups; (b) sonication during reduced reaction. The carboxylate groups on the surface of functionalized MWNTs apparently serve as anchor sites for the metallic nanoparticles. Therefore, the metallic nanoparticles can uniformly distribute onto the surface of c-MWNTs via chemical bonding with the carboxylate as COO(M) or with the O atom of an ester-like form as C(=O)CO(M).[26] If MWNTs are not functionalized, no metal nanoparticles can be formed on the nanotube surface after sonication because the metallic nanoparticles would fall off from the surface of MWNTs during sonication due to the weak physical adsorption. Besides functionalized group, sonication plays an important role in synthesis of c-MWNTs-supported metallic nanoparticles catalysts. It is known that ultrasonic vibrations can produce tremendous creation/oscillation rates of bubbles and transient high temperatures inside hot spots that could cause dispersion of particles and reduce particles in size.[23,27] When the system is only mechanically stirred without sonication, the resulted nanoparticle sizes were very large and clumped together, which is discussed in our previous paper.[25]

The representative TEM images of Pt/c-MWNT, Ru/c-MWNT and bimetallicPtRu/c-MWNT catalysts ate shown in Fig. 1(a-c), respectively. These metallic nanoparticles are uniformly dispersed on the surface of c-MWNT supports. The nanoparticle size were measured using counting at least 200 particles from enlarged TEM

images by imaging analysis software, Matrox Inspector (Matrox Electronic Systems Ltd). A description of determining the size and standard deviation of nanoparticles using the imaging analysis software is described in our previous paper. Fig.1 (d-f) showed the size distribution histograms of Pt/c-MWNT, Ru/c-MWNT and bimetallicPtRu/c-MWNT catalysts, respectively. The average particle size distributions determined from imaging analysis are given as follows: Pt/c-MWNTs (3.1 ± 0.7 nm) (Fig. 1d), Ru/c-MWNTs (5.8 ± 1.0 nm) (Fig. 1e) and PtRu/c-MWNTs (1.9 ± 0.33 nm) (Fig. 1f).

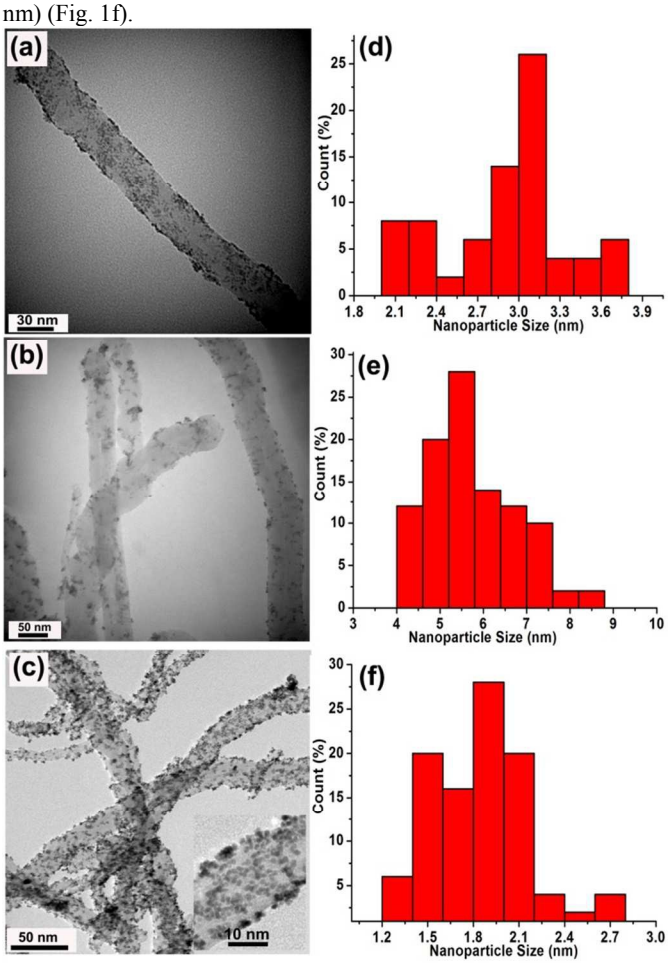

Fig. 1. TEM images and nanoparticles size distribution for Pt/c-MWNTs (a, d), Ru/c-MWNTs (b, e) and PtRu/c-MWNTs (c, f), the insert of (c) shows the HRTEM image of PtRu/c-MWNTs.

The prepared PtRu/c-MWCNTs nanocomposites were also characterized by X-ray diffraction (XRD), together with the patterns of the Pt/c-MWCNTs and Ru/ c-MWCNTs nanocomposites, as shown in Fig. 2. The first diffraction peak at around $2\theta = 26.2^{o}$ is due to the (002) diffraction of the graphitic carbon of MWNTs. The XRD pattern of Pt/c-MWNTs showed the four typical diffraction peaks at the Bragg angles of 39.9^{o} and 46.2^{o}, correspond to the (111) and (200) crystalline planes of the face-centered cubic (fcc) structure of the Pt (Fig. 2a). For the Ru/c-MWNTs product (Fig. 2b), only (111) crystal planes at around $2\theta = 42.3^{o}$, respectively, can be found, demonstrated the Ru nanoparticles have a hexagonal close-packed (hcp) structure. Fig. 2c showed the XRD pattern of the PtRu/c-MWNTs nanocomposites. A shift in this Pt peak position toward the higher angle can be seen clearly for PtRu/c-MWNTs nanocomposites, which indicating formation of an alloy phase between Pt and Ru.[28] In addition, diffraction peak near 42.3^{o} in 2θ from Ru is not observed, which further proved that Ru could possibly enter the Pt lattice and formed the PtRu alloy in the nanocomposites.[29] According to our previous research, the PtRu/c-MWNTs nanocomposites synthesized by the ultrasonic method are most likely having a random alloy structure.[30] The average alloy particle sizes of the PtRu/c-MWNTs was calculated using the Scherer equation:[30]

$$L = \frac{0.9\,\lambda_{K\alpha 1}}{B_{2\theta}\cos\theta_{\max}}$$

where L is the mean size of PtRu alloy particles, $\lambda_{K\alpha 1}$ is the X-ray wavelength (λ=1.5418 Å), θ_{max} is the angle of the peak, and $B_{2\theta}$ is the half-peak width. Average size of PtRu alloy nanoparticles calculated from that equation is 1.87 nm, which is in good agreement with that determined from TEM, indicating good crystallinity and dispersion of the supported alloy nanoparticles.

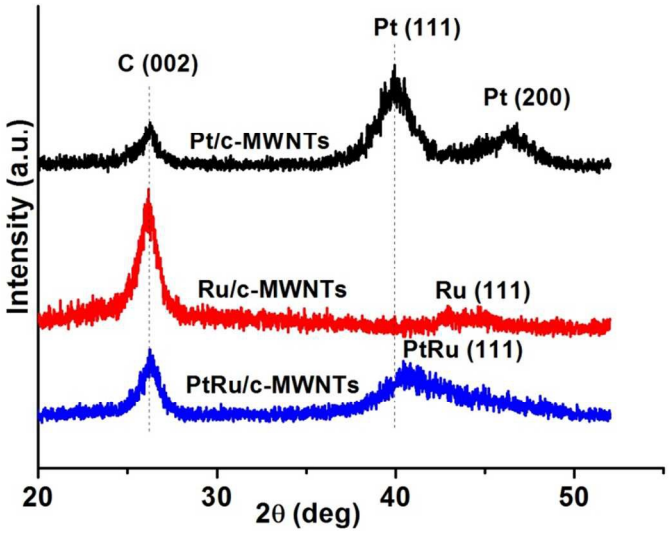

Fig. 2. XRD patterns of Pt/c-MWNTs, Ru/c-MWNTs and PtRu/c-MWNTs.

To further validate the formation of PtRu/c-MWNTs, the components of this composite were investigated with energy dispersive X-ray spectroscopy (EDX) analysis (Fig. S1†). As shown in Fig. S1c, C, Pt and Ru elements were evidently detected, wherein the semiquantitative analysis showed that the atomic ratio between Pt and Ru elements is approximately 1:1. In addition, ICP-AES analysis was used to further investigate the loading of the nanoparticles in the nanocomposites. The mass of Pt in the Pt/c-MWNTs nanocomposites is 16.1 wt.% and that Ru in the Ru/c-MWNTs nanocomposites is 9.2 wt.%. However, the mass of Pt and Ru elements in the PtRu/c-MWNTs nanocomposites decreased to 8.0 wt.% and 4.2 wt%, respectively, corresponding to approximately a 1 : 1 molar ratio of Pt : Ru in the nanocomposites.

X-Ray photoelectron spectroscopy (XPS) characterization was carried out to explore the structures of PtRu/c-MWNTs nanocomposites. The survey XPS spectra of Pt/c-MWNTs, Ru/c-MWNTs and PtRu/c-MWNTs nanocomposites were shown in Fig. S2 (See Supporting Information). Fig. 3a showed the C1s XPS spectrum of c-MWNTs in the nanocomposites. The clear peak appeared at *ca*. 290.6 eV was assigned to carbonyl (HO-C=O), which was attributed with the functionalization by carboxylate groups. Fig. 3b showed the Pt 4f spectrum of PtRu/c-MWNTs nanocomposites. The Pt 4f spectrum consists of two individual peaks at approximately *ca*. 71.3 eV and 74.7 eV, which can be attributed to

Pt 4f $_{7/2}$ and Pt 4f $_{5/2}$ binding energies, respectively.[31] These two bands could be further deconvoluted into two peaks, respectively,

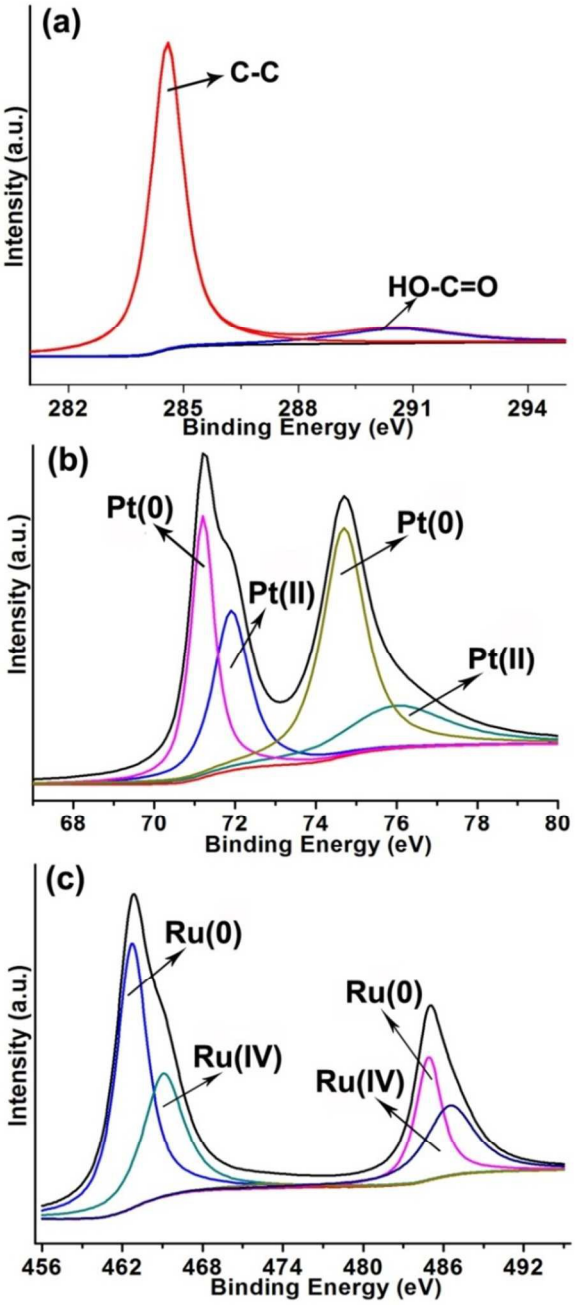

Fig. 3. XPS spectra of PtRu/c-MWNTs. (a) C 1s, (b) Pt 4f and (c) Ru 3p.

at *ca*. 71.2, 71.9 eV and 74.7, 76.0 eV. The bands at *ca*. 71.2 and 74.7 eV are attributed to metallic Pt (0). Those at *ca*. 71.9 and 76.0 eV are ascribed to the Pt (II) species such as PtO, which could be due to the slight oxidation of Pt nanoparticles upon exposure to air. The calculated surface percentages of the metallic Pt (0) and Pt (II) in PtRu/c-MWNTs nanocomposites were 61.4% and 38.6%, respectively, which indicated metallic Pt (0) is the predominant species in the nanocomposites. As for the Ru 3p peaks (Fig. 3c), the component peaks at *ca*. 462.7 and 484.9 eV could be assigned to metallic Ru (0).[21] Those at *ca*. 465.1 and 486.5 eV could be assigned to Ru (IV). The high calculated surface percentages of the Ru (IV) (42.8 %) in the Ru XPS spectrum could be explained considering the formation of RuO_2 because of partially oxidizing metallic Ru. This value is in agreement with data already reported in the literatures.[21] Furthermore, the XPS analysis demonstrated that the molar ratio between Pt and Ru in the bimetallic PtRu is approximately 1 : 1, which is high agreement with EDX and ICP-AES analysis.

3.2 Electrochemical Characterization of PtRu/c-MWNTs catalyst

Electrochemical active surface area (ECSA) was first used to demonstrate the electrochemical performance of PtRu/c-MWNTs catalyst. Fig. 4a shows the cyclic voltammograms (CVs) of Pt/c-MWNTs, PtRu/c-MWNTs and commercial Pt/C (20 wt.%) catalysts in N_2-saturated 0.5 M H_2SO_4 solution at room temperature at a scan rate of 100 mV s^{-1}. ECSA of catalysts can be calculated by measuring the charge collected in the hydrogen adsorption/desorption region after double-layer correction (-0.27-0.13 V) (Table 1). It is found that the ECSA value of PtRu/c-MWNTs (133.2 m^2 g_{Pt}^{-1}) is much higher than those of Pt/c-MWNTs (72.2 m^2 g_{Pt}^{-1}), commercial Pt/C (55.6 m^2 g_{Pt}^{-1}), and recent state-of-art Pt-based nanomaterials such as Ag@Pt/C (75.8 m^2 g_{Pt}^{-1}),[32] Pd nanohollows/Pt nanorods core/shell composites (80.6 m^2 g_{Pt}^{-1}),[33] Pt-Ru/vertically oriented graphene catalyst (260 cm^2 mg_{Pt}^{-1}) *etc*.[34] (Fig. 4b). This result reveals that the PtRu/c-MWNTs catalyst has a high electrocatalytic activity, which can be attributed to the bimetallic structure, small particle size and the uniform distribution of PtRu nanoparticles on c-MWNTs. This strongly suggests that PtRu/c-MWNTs catalyst is electrochemically more accessible, which is of great importance for electrocatalytic reactions.

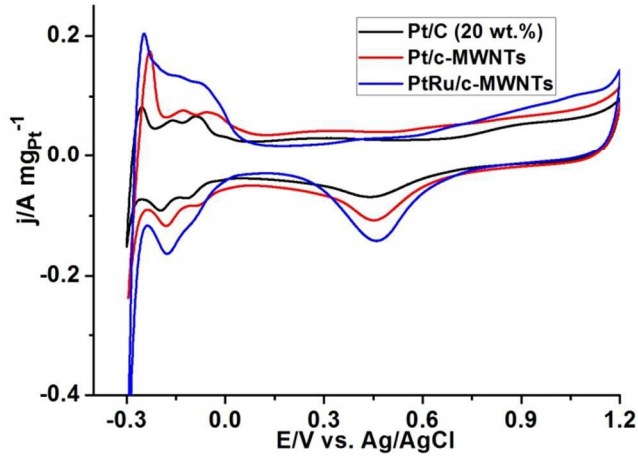

Fig. 4. CVs of PtRu/c-MWNTs, Pt/c-MWNTs and commercial Pt/C (20 wt.%) catalysts modified GC electrodes in a N_2-sparged 0.5 M H_2SO_4 solution at the scan rate of 100 mV/s.

Methanol was used as a model molecule to study the electrocatalytic performance of PtRu/c-MWNTs catalyst. Fig. 5a shows the CVs of glassy carbon (GC) electrodes modified by PtRu/c-MWNTs, Pt/c-MWNTs and commercial Pt/C catalysts in a 0.5 M H_2SO_4 solution containing 0.5 M methanol. The forward oxidation peak (I_f) and the backward oxidation peak (I_b) occurring at 0.68 V and 0.53 V for commercial Pt/C (20 wt.%), 0.65 V and 0.46 V for Pt/c-MWNTs, and 0. 64 V and 0.43 V for PtRu/c-MWNTs catalysts are observed (vs. Ag/AgCl). The mass current density for methanol oxidation in PtRu/c-MWNTs catalyst (1236.0 mA mg_{pt}^{-1}) was calculated to be 2.87 and 5.77 times higher than those of Pt/c-MWNTs (431.3 mA mg_{pt}^{-1}) and commercial Pt/C (20 wt. %) catalyst (214.2 mA mg_{pt}^{-1}), respectively (Fig. 5a and Table 1). Furthermore, the specific activity

of catalysts normalized by the ECSA value by was also used to reveal their electrochemical performance (Table 1). The current density of PtRu/c-MWNTs catalyst (1.4 mA cm^{-2}) is higher than those of Pt/c-MWNTs (0.6 mA cm^{-2}) and Pt/C (20 wt.%) (0.42 mA cm^{-2}), respectively. Fig. 5b shows the linear sweep voltammetry curves (LSVs) of PtRu/c-MWNTs and commercial Pt/C (20 wt.%) catalysts. It is found that the corresponding potential on PtRu/c-MWNTs is much lower than that on commercial Pt/C (20 wt.%) catalyst at a given oxidation current density. It reveals the PtRu/c-MWNTs have better electrochemical performance for methanol oxidation than the commercial Pt/C catalyst at all applied potential. Therefore, all the above results indicate that the PtRu/c-MWNTs catalyst exhibit much enhanced electrocatalytic activity for methanol oxidation reaction, which is probably attributed to three main factors: (i) The bimetallic PtRu nanoparticles could produce high ECSA, which leads to the high electrocatalytic activity; (ii) The PtRu nanoparticles in nanocomposites with small size and uniform particle distribution synthesized using the sonichemical method exhibit higher electroactivity than that with the bigger size; and (iii) good dispersion of bimetallic PtRu nanoparticles with small size on the MWNTs with the large surface area could provide many active sites and result in high electrocatalytic activity.

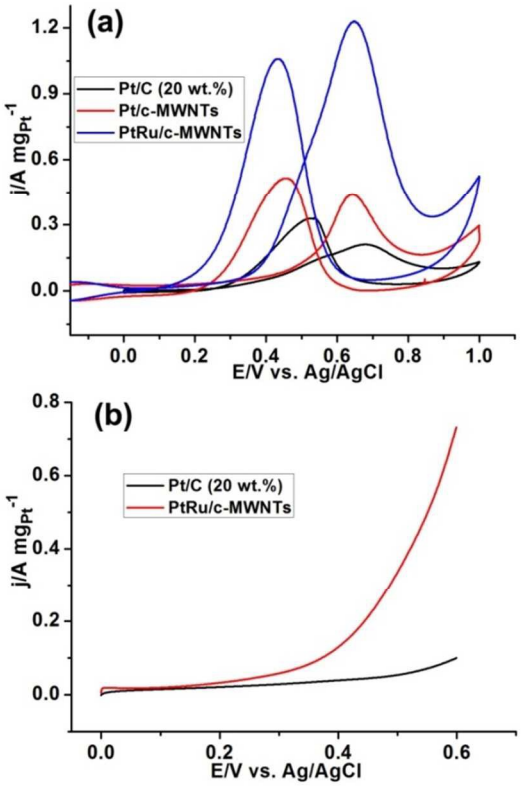

Fig.5. (a) CVs of PtRu/c-MWNTs, Pt/c-MWNTs and commercial Pt/C (20 wt.%) catalysts, and (b) LSVs of PtRu/c-MWNTs and commercial Pt/C (20 wt.%) catalysts modified GC electrodes in a N_2-sparged 0.5 M H_2SO_4 solution containing 0.5 M methanol at the scan rate of 50 mV/s.

The catalyst tolerance and stability of catalyst are very important issues for fuel cell. As shown in Fig. 5a and Table 1, the ratio of the I_f to I_b (I_f/I_b) of PtRu/c-MWNTs catalyst is 1.25, which is higher than those of the Pt/c-MWNTs catalyst (0.86) and the commercial Pt/C (20 wt.%) catalyst (0.64). The higher ratio reveals the PtRu/c-MWNTs catalyst has more effective removal of the poisoning species such as CO on the catalyst surface, which leads to a better tolerance. CO-stripping experiments provide additional information on the surface mobility of CO. Fig. 6a shows the CO stripping voltammograms for the synthesized PtRu/c-MWNTs and commercial Pt/C catalysts. The PtRu/c-MWNTs catalyst shows the much lower onset potential (0.43 V) of CO stripping compared with that of the commercial Pt/C catalyst (0.67). The lower onset potential of PtRu/c-MWNTs indicates easier removal of CO_{ad} from the catalyst, which would enhance its activity for methanol oxidation. It is well known that the introduction of Ru in Pt-based catalysts promotes the oxidation of CO, which is produced as intermediate during the methanol oxidation reaction. Additionally, significant amount of RuO_2 was found in PtRu/c-MWNTs catalyst (42.8 %), which also can promote the oxidization of CO by forming Ru−OH on the surface.

Table 1. Catalyst Characterization and Catalytic Performance Characteristics of PtRu/c-MWNTs, Pt/c-MWNTs and commercial Pt/C (20 wt.%) catalysts.

Catalyst	PtRu/c-MWNTs	Pt/c-MWNTs	Pt/C (20 wt.%)
ECSA (m^2 gPt^{-1})	133.2	75.2	62.6
$I_{m\text{-}peak}$ (mA mg_{Pt}^{-1})[a]	1236.0	431.3	214.2
$I_{m\text{-}peak}$ (mA cm^{-2})[b]	1.4	0.6	0.4
I_f/I_b	1.25	0.86	0.64

[a]Mass activities, [b]Specific activities $I_{m\text{-}peak}$, determined at the peak potential and in the condition of 0.5 M H_2SO_4 solution containing 0.5 M methanol.

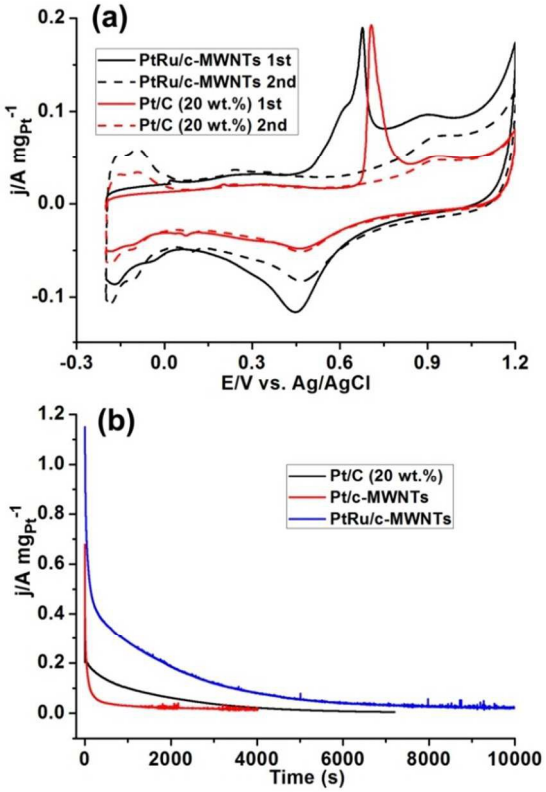

Fig. 6. (a) CO stripping curves of the synthesized PtRu/c-MWNTs and commercial Pt/C catalysts at a scan rate of 50 mV s^{-1} in 0.5 M H2SO4solution. (b) I−t curves of the PtRu/c-MWNTs, Pt/c-MWNTs and commercial Pt/C (20 wt.%) catalysts modified on GC electrodes at 0.6 V in a N_2-sparged 0.5 M H_2SO_4 solution containing 0.5 M methanol.

The long term performance of PtRu/c-MWNTs catalyst toward methanol oxidation reaction was used for studying its

stability, and the Pt/c-MWTNs and commercial Pt/C (20 wt.%) catalysts were employed as comparisons. The corresponding i−t curves are shown in Fig. 6b. It can be clearly seen that the oxidation current of PtRu/c-MWNTs catalyst is much higher than those of Pt/c-MWNTs and commercial Pt/C (20 wt.%) catalysts in the entire time range, and the current density decay of PtRu/c-MWNTs catalyst is also the slowest among in these three catalysts. The oxidation current density of PtRu/c-MWNTs catalyst at 10000 s is 22.5 mA mg_{Pt}^{-1}. The long-term cycle stabilities of the PtRu/c-MWNTs and commercial Pt/C electrodes for methanol oxidation were also studied, which can be seen in Fig. S3†. In the case of PtRu/c-MWNTs catalyst, the forward peak currents density after 500 cycles is about 83.7 % of that measured at the first cycle. However, for commercial Pt/C catalyst, a large loss (39.7 %) is found. The observations imply that the PtRu/c-MWNTs catalyst possesses significantly enhanced long-term cycle stability for methanol oxidation in the acid media.

4. Conclusions

In summary, a facile and one-step ultrasonic assisted synthesis method has been employed to synthesize the PtRu/c-MWNTs catalyst. The bimetallic PtRu nanoparticles with ultrasmall size, uniform distribution and atomic Pt:Ru ratio of 1:1 adhere to the surface of c-MWNTs exhibit an enhanced electrochemical performance toward methanol oxidation. It is found that this catalyst has much higher electrochemical active surface area (ECSA) (133.2 m^2 g_{Pt}^{-1}) than those of Pt/c-MWNTs (72.2 m^2 g_{Pt}^{-1}) and commercial Pt/C (20 wt.%) (55.6 m^2 g_{Pt}^{-1}). The mass current density for methanol oxidation in PtRu/c-MWNTs catalyst (1236.0 mA mg_{pt}^{-1}) was calculated to be 2.87 and 5.77 times higher than those of Pt/c-MWNTs (431.3 mA mg_{pt}^{-1}) and commercial Pt/C (20 wt. %) catalyst (214.2 mA mg_{pt}^{-1}), respectively. Furthermore, outstanding tolerance to CO poisoning and stability toward methanol oxidation were also exhibited by this catalyst. Importantly, the low Pt loading in catalyst (8 wt.%) and enhanced electrocatalytic activity suggest the PtRu/c-MWNTs nanocomposite is an excellent catalyst for methanol oxidation.

Acknowledgements

We gratefully acknowledge the financial support from a WSU start-up grant. J Y and XC acknowledge the funding from National Science Foundation of China (50902061). Additionally, Y.Z would like to thank the Scientific and Technical Innovation Project for Graduate Students (CXZZ13_0664).

Notes and references

[a] School of Materials Science and Engineering, Jiangsu University, Zhenjiang, 212013, Jiangsu, PR China.
E-mail: yangjuan6347@mail.ujs.edu.cn
[b] School of Mechanical and Materials Engineering Washington State University, Pullman, WA 99164-2920, United States
E-mail: Yuehe.lin@wsu.edu
[c] Department of Chemistry, University of Idaho, Moscow, Idaho 83844-2343, United States.
‡These authors contributed equally to the work.

Electronic Supplementary Information (ESI) available: EDX and XPS spectra of Pt/c-MWNTs, Ru/c-MWNTs and PtRu/c-MWNTs. See DOI: 10.1039/b000000x/

1 N. Kakati, J. Maiti, S. H. Lee, S. H. Jee, B. Viswanathan and Y. S. Yoon, *Chem. Rev*., 2014, **114**, 12397-12429.
2 Y. Lin, X. Cui, C. Yen, C. M. Wai, , Langmuir, 2005, 21, 11474-11479.
3 a). S. K. Kamarudina, F. Achmada and W. R. W. Dauda, *Int. J. Hydrogen Energy*, 2009, **34**, 6902-6916; b). S. Zhang, Y. Shao, G. Yin, Y. Lin, J. Mater. Chem. A, 2013, 1, 4631-4641.
4 A. S. Aricò, S. Srinivasan and V. Antonucci, *Fuel Cells*, 2001, **1**,133–161.
5 K. Sundmacher, T. Schultz, S. Zhou, K. Scott, M. Ginkel and E. D. Gilles, *Chem. Eng. Sci*., 2001, 56, 333-341.
6 H. Liu, C. Song, L. Zhang, J. Zhang, H. Wang and D. P. Wilkinson, *J. Power Sources.,* Volume 155, Issue 2, 21 April 2006, Pages 95–110
7 S. Zhou, T. Schultz, M. Peglow and K. Sundmacher, *Phys. Chem. Chem. Phys*., 2001, 3, 347-355.
8 J. Zhao, X. He, J. Tian, C. Wan and C. Jiang, *Energy Convers. Manage*., 2007, **48**, 450-453.
9 B. D. McNicol, D. A. J. Rand and K. R. Williams, *J. Power Sources*, 1999, **83**, 15-31.
10 S. Chauhan, G. J. Richards, T. Mori, P. Yan, J. P. Hill, K. Ariga, J. Zou and J. Drennan, *J. Mater. Chem. A*, 2013, **1**, 6262-6270.
11 a) M. E. Scofield, C. Koenigsmann, L. Wang, H. Liu and S. S. Wong, E*nergy Environ. Sci*., 2015, **8**, 350-363;b) C. Zhu, S. Guo and S. Dong, *Adv. Mater.,* 2012, **24**, 2326–2331.
12 a) T. N. Huan, D. V. Shinde, S. Kim, S. H. Han, V. Artero and H. Chung, *RSC Adv*., 2015, **5**, 6940-6944; b) C. Zhu, S. Guo and S. Dong, *Chem. -Eur. J*., 2013 **19**, 1104-1111.
13 T. Y. Chen, G. W. Lee, Y. T. Liu, Y. F. Liao, C. C. Huang, D. S. Lin and T. L. Lin, *J. Mater. Chem. A*, 2015, **3**, 1518-1529.
14 C. Wang, F. Ren, C. Zhai, K. Zhang, B. Yang, D. Bin, H. Wang, P. Yang and Y. Du, *RSC Adv*., 2014, **4**, 57600-57607.
15 Z. Cai, Y. Kuang, X. Qi, P. Wang, Y. Zhang, Z. Zhang and X. Sun, *J. Mater. Chem. A*, 2015, **3**, 1182-1187.
16 D. B. Huang, Q. Yuan, H. H. Wang and Z. Y. Zhou, *Chem. Commun*., 2014, **50**, 13551-13554
17 X. Huang, E. Zhu, Y. Chen, Y. Li, C. Y. Chiu, Y. Xu, Z. Lin, X. Duan and Y. Huang, *Adv. Mate*., 2013, **25**, 2974–2979.
18 Z. Chen, X. Qiu, B. Lu, S. Zhang, W. Zhu and L. Chen, *Electrochem. Commun.,* 2005, **7**, 593-596.
19 Y. J. Gu and W. T. Wong, *J. Electrochem. Soc*., 2006, **153**, A1714-A1718.
20 J. Zheng, D. A. Cullen, R. V. Forest, J. Wittkopf, Z. Zhuang, W. Sheng, J. G. Chen, and Y. Yan. *ACS Catal*., 2015, **DOI:** 10.1021/cs501449y
21 J. C. Calderón, G. García, L. Calvillo, J. L. Rodríguez, M. J. Lázaro, E. Pastor, *Appl. Catal., B*, 2015, **165**, 676–686.
22 J. H. Bang and K. S. Suslick, *Adv. Mater*., 2010, **22**, 1039-1059.
23 J. H. Bang and K. S. Suslick, *J. Am. Chem. Soc*., 2007, **129**, 2242-2243.
24 Y. Li, W. Ding, M. Li, H. Xia, D. Wang and X. Tao, *J. Mater. Chem. A*, 2015, **3**, 368-376.
25 H. B. Pan and C. M. Wai, *J. Phys. Chem. C*, 2009, **113**, 19782-19788.
26 D. Q. Yang and E. Sacher, *J. Phys. Chem. C*, 2008, **112**, 4075-4082.
27 T. J. Mason and J. P. Lorimer, Applied Sonochemistry, Wiley-VCH, Weinheim, Germany, 2001.

28 E. M. Crabb, M. K. Ravikumar, D. Thompsett and M. Hurford, *Phys. Chem. Chem. Phys*., 2004, **6**, 1792-1798.
29 Y. Zhao, X. Yang, L. Zhan, S. Ou and J. Tian. *J. Mater. Chem.*, 2011, **21**, 4257-4263.
30 H. B. Pan and C. M. Wai, *New J. Chem*., 2011, **35**, 1649-1660.
31 K. C. Park, I. Y. Jang, W. Wongwiriyapan, S. Morimoto, Y. J. Kim, Y. C. Jung, T. Toyad and M. Endo, *J. Mater. Chem.*, 2010, **20**, 5345-5354.
32 J. Cao, M. Guo, J. Wu, J. Xu, W. Wang and Z. Chen, *J. Power Sources*, 2015, **277**, 155-160.
33 S. Lai, C. Fu, Y. Chen, X. Yu, X. Lai, C. Ye and J. Hu, *J. Power Sources*, 2015, 274, 604-610.
34 Z. Bo, D. Hu, J. Kong, J. Yan and K. Cen, *J. Power Sources*, 2015, **273**, 530-537.

Table of Contents Entry

.

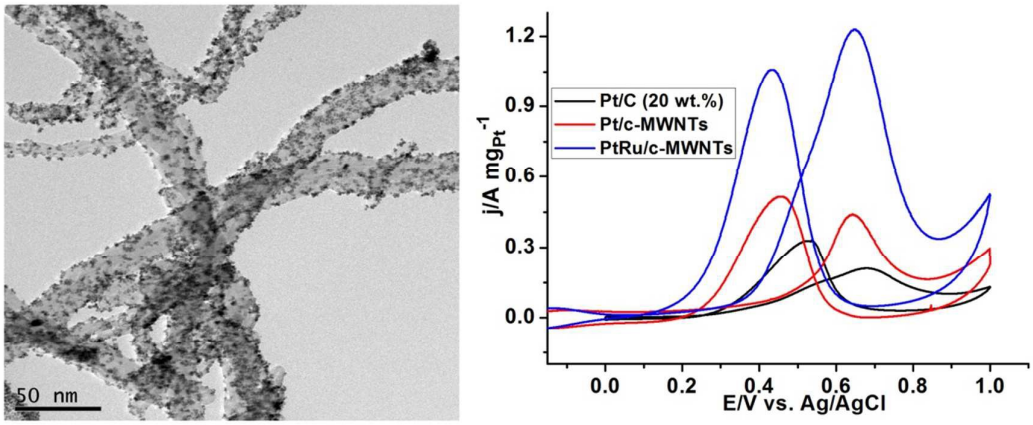

We demonstrate a facile and one-step ultrasonic method to synthesize the PtRu/c-MWNTs catalyst with bimetallic structure, ultrasmall size and uniform distribution. The low mass loading of Pt, but the excellent electrochemical properties demonstrated that it is a favorable electrocatalyst for methanol oxidation.